JCIM JOURNAL OF CHEMICAL INFORMATION AND MODELING

Article

pubs.acs.org/jcim

Multiscale Modeling of Thiol Overoxidation in Peroxiredoxins by Hydrogen Peroxide

J. Semelak,[†] F. Battistini,[‡] R. Radi,[§] M. Trujillo,[§] A. Zeida,[*,§] and D. A. Estrin[*,†]

[†]Departamento de Química Inorgánica, Analítica y Química Física, INQUIMAE-CONICET, Facultad de Ciencias Exactas y Naturales, Ciudad Universitaria, Pab. 2, CP 1428, Buenos Aires, Argentina

[‡]Institute for Research in Biomedicine (IRB Barcelona), The Barcelona Institute of Science and Technology, 08028 Barcelona, Spain

[§]Departamento de Bioquímica and Centro de Investigaciones Biomédicas (CEINBIO), Facultad de Medicina, Av. Gral. Flores 2125, CP 11800 Montevideo, Uruguay

Supporting Information

ABSTRACT: In this work, we employ a multiscale quantum-classical mechanics (QM/MM) scheme to investigate the chemical reactivity of sulfenic acids (RSOH) toward hydrogen peroxide, both in aqueous solution and in the protein environment of the peroxiredoxin alkyl hydroperoxide reductase E from *Mycobacterium tuberculosis* (*Mt*AhpE). The reaction of oxidation of cysteine with hydrogen peroxides, catalyzed by peroxiredoxins, is usually accelerated several orders of magnitude in comparison with the analogous reaction in solution. The resulting cysteine sulfenic acid is then reduced in other steps of the catalytic cycle, recovering the original thiol. However, under some conditions, the sulfenic acid can react with another equivalent of oxidant to form a sulfinic acid (RSO_2H). This process is called overoxidation and has been associated with redox signaling. Herein, we employed a multiscale scheme based on density function theory calculations coupled to the classical AMBER force field, developed in our group, to establish the molecular basis of thiol overoxidation by hydrogen peroxide. Our results suggest that residues that play key catalytic roles in the oxidation of *Mt*AhpE are not relevant in the overoxidation process. Indeed, the calculations propose that the process is unfavored by this particular enzyme microenvironment.

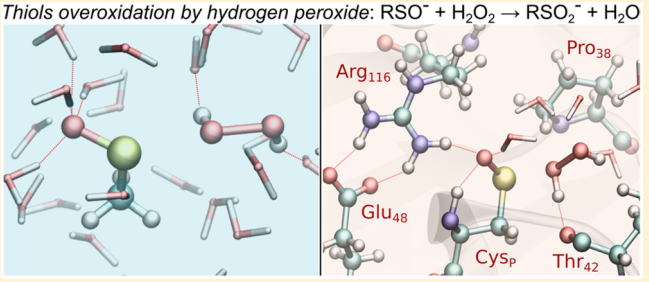

1. INTRODUCTION

Computer simulation techniques provide an excellent tool to shed light on the molecular basis of chemical and biological processes. Specifically, reactive processes in complex environments can be dealt with using multiscale techniques which may be envisaged in two different schemes. One method consists of applying different levels of theory in a sequential way, i.e., using classical atomistic molecular dynamics (MD) simulations followed by quantum mechanics (QM) calculations of a selected part of the system. The other method consists of applying simultaneously the two techniques, considering one part of the system described at one level of theory while the rest is treated at the other level, i.e., the standard hybrid quantum classical techniques (QM/MM).

In our group we have developed two different QM/MM codes; one is based on a numerical DFT scheme coupled to the AMBER force field.[1] Using this method, we have investigated several reactions by computing potential energy profiles and elucidated reaction mechanisms for processes both in solution, such as the chorismate to prephenate conversion,[1] or in protein environments, such as the NO detoxification mechanism catalyzed by truncated hemoglobin N of *Mycobacterium tuberculosis*[2] and the catalytic mechanism and the detection of a novel intermediate in indoleamine 2,3-deoxygenase.[3] The other code, named LIO, is based on a Gaussian basis set approach, has been optimized for running in GPU,[4,5] and has been extensively used for the investigation of reaction mechanisms and selectivity of hydroperoxides with the cysteine catalyzed reaction in peroxiredoxin, as well as in aqueous solution, yielding in both cases the corresponding sulfenic acid (reaction 1). The use of an appropriate combination of classical MD followed by a computationally efficient QM/MM code allowed us to achieve a more extensive sampling of the configurational space and to obtain free energy profiles. The free energy profiles provide information on kinetic and thermodynamics properties that could be compared directly with experimental values, since both thermal and entropic effects are included, which are not considered in potential energy profiles.

Herein, we illustrate the combination of classical MD and QM/MM MD with two reactivity problems in complex environments. In the first place, we analyze the reaction of a

Special Issue: Molecular Simulation in Latin America: Coming of Age

Received: September 19, 2019
Published: November 13, 2019

DOI: 10.1021/acs.jcim.9b00817
J. Chem. Inf. Model. XXXX, XXX, XXX−XXX

model sulfenic acid with hydrogen peroxide in aqueous solution that yields the corresponding sulfinic acid (RSO_2H). [According to their low pK_a values (~2 for free cysteine), these compounds exist mostly under the deprotonated, sulfinate form at physiological pH.[6]] This is an extremely challenging problem due to the dynamical nature of aqueous solvation. In the second place, we analyze the same reaction in another challenging situation, a protein that presents a highly nanoheterogeneous environment.

Cysteine sulfinic acids (Cys-SO_2H) are oxidized forms of either free or protein Cys residues. Free Cys oxidation to sulfinic acid, catalyzed by Fe^{2+}-dependent Cys dioxygenases, is the first step in the catabolic route of the amino acid.[6] In turn, protein Cys-SO_2H, initially considered an oxidative post-translational modification arising mostly as an artifact from purification processes, is now known to occur *in vivo*, in different proteins.[7,8] Indeed, quantitative analysis estimated that Cys-SO_2H accounts for ~1−2% of total Cys residues in the soluble proteins of the rat liver.[9] The formation of sulfinic acid can involve two consecutive two-electron oxidations of thiolates (RS^-): the first yielding a sulfenate (RSO^-; reaction 1), which is then further oxidized to sulfinate (RSO_2^-; reaction 2), in a process that is often referred to as over- or hyperoxidation.[10,11]

$$RS^- + R'OOH \rightarrow RSO^- + R'OH \qquad \text{(reaction 1)}$$

$$RSO^- + R'OOH \rightarrow RSO_2^- + R'OH \qquad \text{(reaction 2)}$$

Alternatively, sulfinic acid could result from the one-electron oxidation of thiolates to thiyl radicals ($RS^\bullet$) followed by a reaction with oxygen, reorganization of the corresponding thioperoxyl radical ($RSOO^\bullet$) to a sulfonyl radical ($RS(O)O^\bullet$), which can eventually be reduced to sulfinic acid.[12−14] Among all the biologically relevant two-electron oxidants involved in overoxidation reactions, hydrogen peroxide (H_2O_2) has a recognized role in redox signaling processes.[15,16] The kinetics of the reaction of H_2O_2 with free cysteine and other aliphatic low molecular weight (LMW) thiols is pH-dependent, since pH affects thiolate availability depending on thiol acidity.[17] In addition, pH-independent rate constants are higher—usually in the 10^1 M^{-1} s^{-1} range at 25 °C—for those thiolates of higher basicity, according to their higher nucleophilicity.[18]

In the case of cysteine residues, the protein microenvironment can largely affect reactivity. Among the proteins susceptible to cysteine modification to sulfinic acid (see Table 1 for examples and determined rate constants), peroxiredoxins (Prxs) deserve particular attention. These enzymes catalyze the two-electron reduction of hydroperoxides such as hydrogen peroxide, organic hydroperoxides, and peroxynitrite by ping-pong bisubstratic kinetic mechanisms.[19−21] In the oxidizing part of the catalytic cycle, the peroxidatic cysteine of Prxs (Cys_P) performs the nucleophilic attack on the hydroperoxide yielding the corresponding alcohol as the first product, while the peroxidatic thiol (Cys_P-SH) is oxidized to sulfenic acid (Cys_P-SOH). The oxidation of peroxidatic thiols in Prxs by hydroperoxides is usually very rapid (10^4 to 10^8 M^{-1} s^{-1}).[12,22] Unfortunately, due to the instability of aliphatic LMW sulfenic acids, experimental determinations of the rate constants of their overoxidation are almost lacking.[23−25] pH profile of H_2O_2-mediated protein Cys-SOH oxidation indicated sulfenate as the reactive species,[26] in agreement with computational results.[27] In 2-Cys Prxs there is a resolution step in which CysP-SOH reacts with the resolving Cys (Cys_R) to form a disulfide bond. The latter is then reduced by thioredoxin or a related enzyme. In 1-Cys Prxs, Cys_P-SOH is reduced to Cys_P-SH by different mechanisms, depending on the particular enzyme.[19] Prxs are prone to inactivation by oxidizing substrates, through the reaction of a second hydroperoxide moiety with Cys_P-SOH yielding Cys_P-SO_2H.[28] Prxs overoxidation second-order rate constants are usually ~10^3 times lower than the oxidation ones considering the same hydroperoxide.[29−31] The susceptibility of different Prxs to oxidative inactivation depends on how rapidly overoxidation occurs with respect to other possible pathways of Cys_P-SOH. In particular, overoxidation competes with resolution in 2-Cys Prxs,[32] or with mixed disulfide formation with other cellular thiols both in two-cysteine and 1-Cys Prxs.[32] Sulfinylation can promote protein ubiquitination and degradation by the proteasome.[33] Furthermore, Cys_P-SO_2H in some Prxs can be reduced back to Cys_P-SOH by sulfiredoxins, ATP-dependent enzymes which have been recently reported to also catalyze the reduction of other sulfinylated proteins.[7,34] The reversible inactivation of Prxs due to sulfinylation and reactivation through sulfiredoxin is the basis of the floodgate hypothesis of redox signaling.[32]

In many Prxs, redox changes are associated with changes in their quaternary structures, which importantly affect the enzyme function[35−37] and can also affect the susceptibility to overoxidation.[38,39] In turn, overoxidation of some Prxs promotes the formation of higher molecular weight complexes which acquire chaperone activity.[40]

In this work, we employed a combination of classical MD and QM/MM schemes to describe the molecular basis of Cys_P overoxidation in atomistic detail, choosing as a member of the peroxiredoxin (Prx) family the 1-Cys alkyl hydroperoxide reductase E from *Mycobacterium tuberculosis* (*Mt*AhpE, see Figure 1). This enzyme is dimeric and reduces different hydroperoxides using either mycothiol/mycoredoxin-1 or hydrogen sulfide as a reducing substrate.[26,29,41−43] When the protein is oxidized, it is also dimeric at least during short incubation times (minutes). *Mt*AhpE Cys_P-SOH is relatively stable, its pK_a is 6.6 at 25 °C and its rate constant of H_2O_2-mediated overoxidation is 42 M^{-1} s^{-1} at 25 °C.[26] We present a detailed description of the multiscale simulations approach to investigate this chemical process both in aqueous solution and in the protein environment and correlate our results with experimental findings.

Table 1. Bimolecular Rate Constants of Protein Cys Overoxidation by Hydrogen Peroxide

protein	k' (M^{-1} s^{-1})	conditions	references
human Prx1	1770	pH 7.4; 25 °C	44
	57	pH 7. 0; 30 °C	45
human Prx2	1970	pH 7.4; 25 °C	44
	6000	pH 7.4; 25 °C	46
human Prx3	1100	pH 7.8; 14 °C	47
	6000	pH 7.4; 25 °C	46
M. tuberculosis AhpE	40	pH 7.4; 25 °C	26
human serum albumin	0.4	pH 7.4; 37 °C	48
Cdc25B phosphatase	60	pH 7.0; 20 °C	49
Cdc25C phosphatase	110	pH 7.0; 20 °C	49
S. faecalis NADH peroxidase	0.14	pH 7.0; 25 °C	50
	0.11	pH 7.0; 25 °C	51

DOI: 10.1021/acs.jcim.9b00817
J. Chem. Inf. Model. XXXX, XXX, XXX−XXX

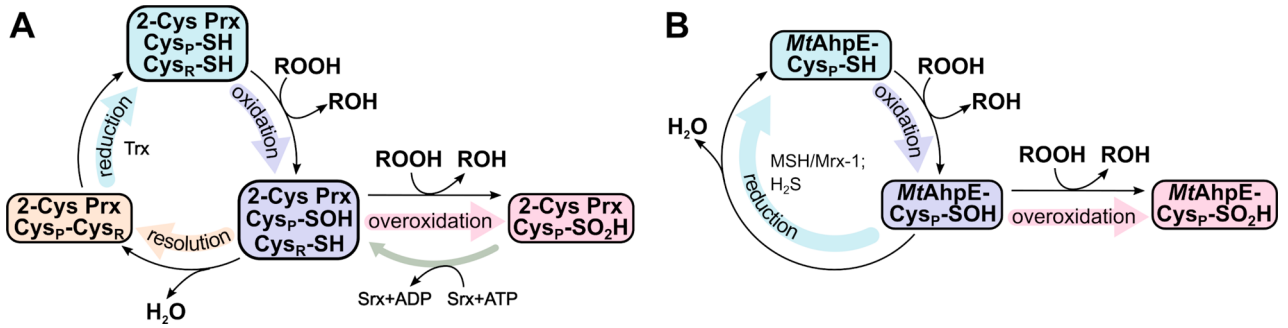

Figure 1. Catalytic cycle of 2-Cys Prxs and *Mt*AhpE. After oxidation of Cys_P to sulfenic acid (violet), the possibility of overoxidation to sulfinic acid by a second hydroperoxide molecule is represented (pink). In 2-Cys Prxs (A), overoxidation competes with enzyme resolution (orange) followed by reduction (cyan) mostly relying on thioredoxin (Trx). In some eukaryotic 2-Cys Prxs, sulfiredoxins (Srx) may reduce the sulfinic acid back to sulfenic acid at the expense of ATP. For *Mt*AhpE (B), two reduction pathways need to be recognized, mycothiol/mycoredoxin-1 (MSH/Mrx-1) or hydrogen sulfide (see the text).

2. METHODS

The oxidation of the model system methanesulfenate ($MeSO^-$) by H_2O_2 was studied employing electronic structure calculations *in vacuo*. We then performed QM/MM simulations to study the reaction of $MeSO^-$ in aqueous solution and *Mt*AhpE-Cys_P-SO^- with H_2O_2. In each case, QM/MM simulations were performed by describing the solvent water molecules at the MM level of theory, and key atoms of reactants were selected to constitute the QM subsystem. $MeSO^-$ and H_2O_2 were treated entirely as quantum residues while only the methylene and $-SO^-$ of the Cys_P (Cys45) were considered in the case of *Mt*AhpE. A detailed description of the protocols employed is given in the next subsections.

2.1. Molecular Dynamics Simulations. Classical molecular dynamics (MD) simulations of the *Mt*AhpE dimer were performed for the thiolate form of the reduced enzyme (*Mt*AhpE-S^-) and for the sulfenate form (*Mt*AhpE-$S0^-$). The X-ray crystal structures of the enzyme in both states were retrieved from the Protein Database (PDB). Two original structures (PDB ID: 1XXU and 1XVW)[52] and their reviewed version by using a new refinement algorithm specially developed for sulfur H-bonds in proteins (PDB ID: 4X0X and 4X1U) were considered.[53] We performed relatively long MD simulations starting from the four structures described above, but nonsignificant differences were observed between the original and the revised structures (see Supporting Information Figure S1). We decided to continue the simulations and analyses using the more recently reported structures.[53]

The four initial models were studied using the same MD protocol. Each system was solvated with an octahedral box of 12 Å in radius with TIP3P water molecules.[54] Protein parameters correspond to the parm14SB Amber force field[55] with the exception of the parameters for the Cys-SO^- residue that were developed using standard protocols.[56] Simulations were performed using periodic boundary conditions with a 10 Å cutoff and particle mesh Ewald summation method for treating the electrostatic interactions. The hydrogen bond lengths were kept at their equilibrium distance by using the SHAKE algorithm,[57] while temperature and pressure were kept constant with a Langevin thermostat[58] and barostat,[59] respectively, as implemented in the AMBER14 program. Each system was minimized in 1000 steps (10 with steepest descent and the rest with conjugate gradient). It was then heated from 0 to 300 K for 20 ps at constant pressure, with a Berendsen thermostat,[60] and pressure was equilibrated at 1 bar for 5 ps. After these two steps, a 10 ns MD long simulation at constant temperature (300 K) and constant volume was performed followed by an unrestrained 700-ns-long production MD at the NPT ensemble.

In order to study the overoxidation process, after characterization of the equilibrium properties of the different systems, a H_2O_2 molecule was placed at the active site of the Cys_P-SO^- system (4X1U) by replacing a water molecule close to Cys_P present in the X-ray crystal structure. A 1-μs-long MD simulation was performed keeping the distance between a peroxide oxygen atom and the sulfur atom less than 4.5 Å. To achieve this, a restraint was applied, such that the external potential on the mentioned distance was null between zero and 4.5 Å and rose sharply to higher values from 4.5 Å onward (acting as a "wall-like" potential). The parameters used for the H_2O_2 molecule were obtained from previous works.[42,61]

2.2. Initial Survey of the Reaction in Model Systems. All the electronic structure calculations were performed with Gaussian 09.[62] Geometry optimizations at different stages of the reaction were performed at the generalized gradient approximation (GGA) level, using the PBE combination of exchange and correlation functional, with a double-ζ plus polarization (dzvp) Gaussian basis set.[63] In each case, frequency calculations were performed, and entropic contributions were calculated as implemented in the Gaussian 09 suite, which considers a harmonic potential and rigid rotor approximation for vibrations and rotations. The transition state structures were confirmed by performing intrinsic reaction coordinate calculations.[64] Additionally, reactions were studied employing the Møller−Plesset perturbation theory (at the MP2 level) with the dzvp basis to evaluate activation barrier underestimations inherent to pure DFT functionals.[65]

2.3. QM/MM MD: System Initial Equilibration. QM/MM simulations were performed using LIO software, compiled with Amber14, which is particularly efficient due to the use of GPUs for the most consuming part of the calculations.[4,66] In each case, initial structures for the reactants were obtained from ab initio, PBE-level geometry optimizations. The reactants were placed in a truncated 25 Å octahedral box filled with TIP3P model water molecules.[54] Periodic boundary conditions were used, and each box contained only the reactants and approximately 4000 explicit water molecules. The Lennard-Jones parameters (ε and σ) for the quantum

DOI: 10.1021/acs.jcim.9b00817
J. Chem. Inf. Model. XXXX, XXX, XXX−XXX

subsystem atoms were 0.2500, 0.1094, 0.2104, and 0.0157 kcal/mol and 2.000, 1.9080, 1.7210, and 1.4870 Å, for S, C, O, and H, respectively. The system was optimized freezing the classical water molecules and, second, restraining the QM subsystem Cartesian coordinates with a quadratic bias potential using a force constant of 400 kcal/mol Å^2, as implemented in the Amber14 suit. Then, 0.1-ns-long classical thermalization dynamics was performed, heating from 0 to 300 K, keeping the internal motion restraint on the reactant complex (RC). Finally, a reliable thermalization of the solute was ensured by a 1 ps QM/MM MD with an uncoupled Berendsen thermostat,[60] in order to control the local kinetic energy of the relatively small QM subsystem. All dynamics visualizations and molecular drawings were performed with VMD 1.9.1.[67]

2.4. QM/MM MD Simulations: Free Energy Profiles Calculation. *2.4.1. General Aspects and Reaction Coordinate Choice.* Free energy profiles were obtained using the umbrella sampling method, a biased molecular dynamics based method for the calculation of one- or more-dimensional free energy profiles.[68,69] Among the different proposed umbrella sampling strategies,[69] we employed the sampling method in which intermediate steps between two thermodynamic states are covered by a series of windows, at each of which a biased MD simulation is performed. The choice of an adequate reaction coordinate and its representation using an order parameter is an open issue in theoretical chemistry.[70−72] Importantly, this parameter is expected to be the degree of freedom associated with the energetic barrier in the transition process, and it is assumed to ensure that the "effective" potential energy surface does not exhibit barriers, between the initial and the final state, higher than thermal energy. If bonds are being formed or broken through the process, distances concerning the involved atoms should be included in the selected degree of freedom, since it is well-known that the breaking and the formation of bonds are processes which usually exhibit great energetic changes. Once the free energy profile is obtained, it is possible to verify whether the system structure does not exhibit large conformational "jumps" going from one window to another.[73] If so, the selected order parameter is likely adequate and the obtained results are reliable. In our case, the order parameter (ξ) that describes the progress of the processes was defined as a combination of geometric parameters. As stated before, this order parameter is referred to as a reaction coordinate even though it might not be the exact reaction coordinate of the system (i.e., the one-dimensional coordinate that connects reactants and products by the minimum free-energy pathway). In this work, the reaction coordinate is defined in each case under study, given by the difference between the nucleophilic sulfur atom and the electrophilic center (O_R oxygen atom for H_2O_2) distance and the distance between the electrophilic center and the closest atom of the leaving group (O_W oxygen atom for H_2O_2). Atom labels and reaction coordinates definitions are illustrated below.

2.4.2. Windows Thermalization in a Charge-Reparametrization Scheme. Initial structures for subsequent umbrella sampling windows were obtained from a steered QM/MM MD simulation. In each case, the system was conducted from the reactant to products in 25 ps using a force constant of 200 kcal/mol Å^2. As we have shown in a previous work, solvent pattern rearrangements related to charge redistribution during the reaction are not well-sampled on the picosecond scale, and this might lead to overestimation of the free energy barriers obtained.[4] The windows were then carefully equilibrated in order to improve solvation sampling, employing a 10-step cycle which involved a QM/MM recalculation of the classical residue's charges and a 0.1 ns MM MD with an internal motion restraint (force constant of 600 kcal/mol Å^2) in each step. After each MM MD, a QM/MM optimization was performed, and the topology was modified replacing the new calculated charges of the QM subsystem for the next step. This process was iteratively repeated 10 times, summing up to 1 ns of classical MD.

2.4.3. Free Energy Profiles Calculation. Equilibrated structures obtained with the previously described charge reparametrization scheme were used as initial coordinates for each umbrella sampling window. The windows were centered at different reaction coordinate reference values, spaced by 0.1 Å in most of the cases, and it was verified that their distributions overlapped. A quadratic bias potential function (also centered in those reference values) was added to the reaction coordinate in each window, and a 5-ps-long uncoupled thermostat QM/MM MD was generated, followed by a 10 ps long QM/MM production MD using the stochastic Langevin thermostat model in order to get a reliable canonical distribution. Biased probability distributions along the reaction coordinate ($P^b(\xi_i)$) were computed using only Langevin MD data. Unbiased free-energy G of the ith window was then recovered from biased simulations as

$$G(\xi_i) = -RT\ \ln(P^b(\xi_i)) - \frac{k}{2}(\xi_i - \xi_i^{ref})^2 + F_i \quad (1)$$

where T is the temperature (300 K), R is the ideal gas constant, ξ_i^{ref} is the reference value of the window, k is the bias force constant (100−200 kcal/mol Å^2, depending on the window), and F_i is an integration constant that cannot be directly obtained from the MD simulation. As mentioned before, $P^b(\xi_i)$ was directly obtained from the MD simulation. Strictly, since the simulations were performed in the canonical ensemble, eq 1 leads to the Helmholtz free energy. However, for condensed systems, it could be considered practically identical to Gibbs free energy. The complete free energy profiles and statistical errors were finally obtained with the umbrella integration method.[69,74] An illustration of the described methodology is shown in Figure 2.

3. RESULTS AND DISCUSSION

3.1. Structural and Dynamical Behavior of the Enzyme in Different Redox States. The dynamical properties of the *Mt*AhpE dimer in the reduced state and its interaction with different substrates have been investigated in previous works by means of MD simulations[42,43,61] and also by NMR experiments.[75] Nonetheless, the oxidized state (Cys_P-SO^-) has not been studied by dynamical techniques. As predicted by the X-ray structures, the oxidation of Cys_P resulted neither in large scale conformational changes in the enzyme nor in significant changes in its dynamical behavior (Figure 3A and B). In spite of that, an important local active site remodelling is noticed when going from Cys_P-S^- to Cys_P-SO^- states: the interaction network responsible for the oxidation step acceleration, present when the enzyme is reduced,[4,61] gets perturbed by the oxidation of Cys_P. Specifically, the hydrogen bond interaction between Cys_P and Thr42 is not present in the sulfenate state, and Arg116 also softens its association with Cys_P as it interacts much more

DOI: 10.1021/acs.jcim.9b00817
J. Chem. Inf. Model. XXXX, XXX, XXX−XXX

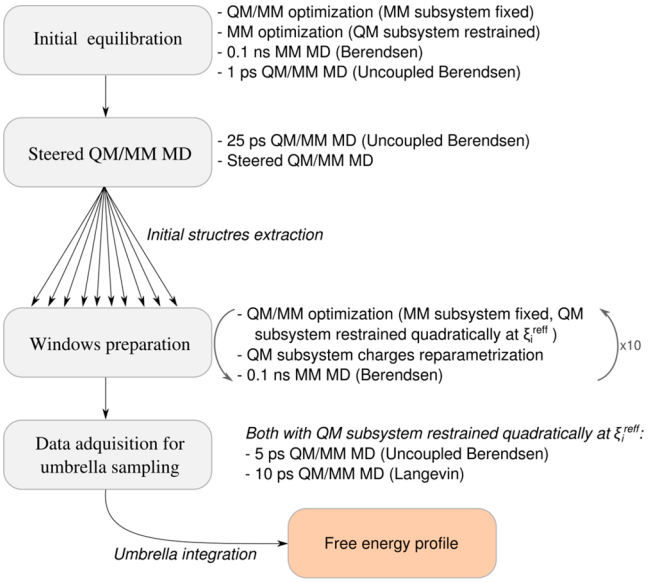

Figure 2. Pipeline representation of the simulation protocol used in this work for obtaining free energy profiles.

strongly with Glu48 (Figure 3C–E). The fact the sulfenate of Cys_P is not particularly stabilized by Thr42 is consistent with the sulfenic acid being less acidic than the thiol in this enzyme.[76] It is worth mentioning that no significant deviations of the C–S–O_S angle (~105–110°) were observed either within the three conformations sampled by classical MD simulations or during QM/MM simulation sampling or the evolution of the reaction (Supporting Information Figure S2), in contrast with the ~153° observed in the case of *Xanthomonas campestris* peroxiredoxin Q sulfenic acid crystals.[77]

These changes affect the positioning of the substrate preceding the overoxidation reaction. When a H_2O_2 molecule is placed at the *Mt*AhpE-Cys_P-SO^- active site, at least three different local conformations could be distinguished (Figure 4A). Two of these conformations (I and II) differ in the hydroperoxide position with respect to Cys_P, with Arg116 interacting directly with both Cys_P and H_2O_2 in conformation II (the most populated conformation within the 1 μs MD simulation) and only with Cys_P in conformation I. The third conformation corresponds to the insertion of H_2O_2 toward the protein core, forcing an to Arg116 shift the active site outward (Figure 4A and Supporting Information Figure S3). As the three conformations showed different properties regarding the

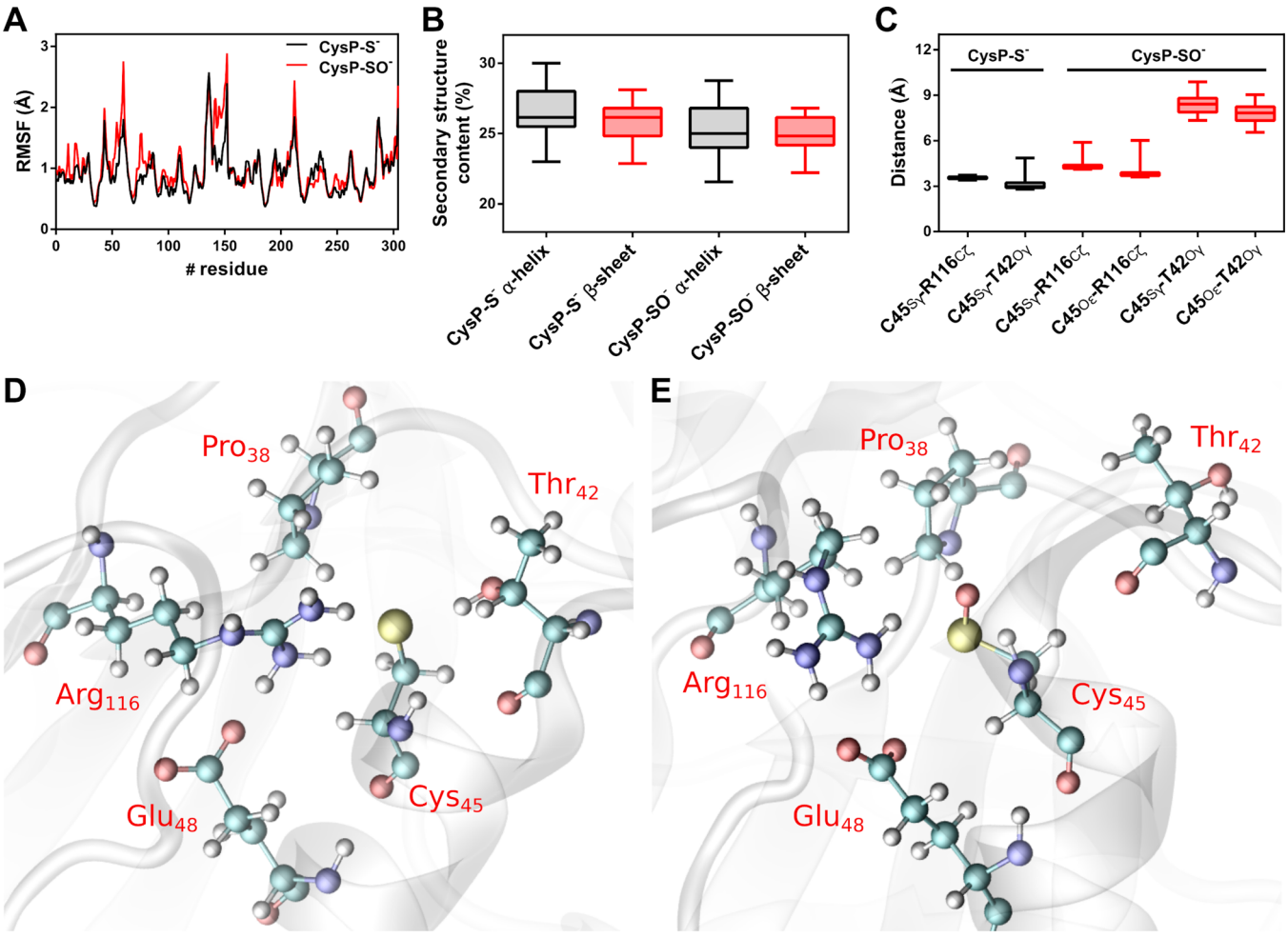

Figure 3. Structural and dynamical comparison of thiolate and sulfenate states of *Mt*AhpE. (A) Root mean square fluctuation (Å) on a per residue basis and (B) secondary structure content (%) obtained from MD simulations of different redox states. (C) Distribution of relevant distances at the active site (Å). (D and E) Typical snapshots of *Mt*AhpE active site taken from MD simulations of Cys_P-S^- and Cys_P-SO^- systems, respectively.

DOI: 10.1021/acs.jcim.9b00817
J. Chem. Inf. Model. XXXX, XXX, XXX–XXX

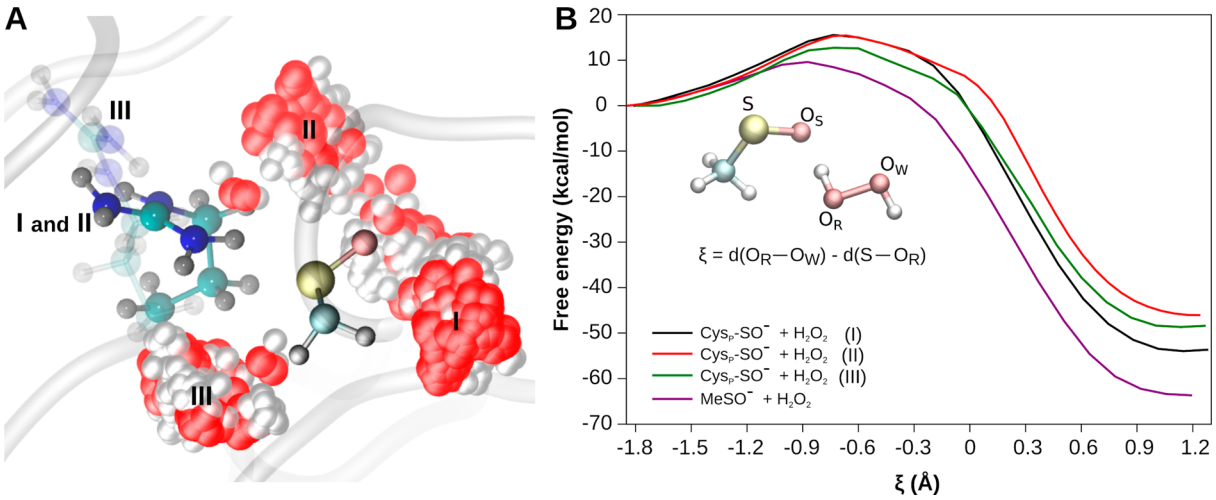

Figure 4. (A) Schematic representation of H_2O_2 sampling in *Mt*AhpE-Cys_P-SO^- active site obtained by restrained MD simulations. Three clusters of H_2O_2 positioning with respect to Cys_P-SO^- were observed (I, II, and III; oxygen and hydrogen atoms density depicted in red and gray, respectively). Two conformations of Arg_{116} are depicted as they depend on H_2O_2 locations. (B) Free energy profiles of H_2O_2 reduction reactions by $MeSO^-$ or Cys_P-SO^- starting from the three different conformations observed in A obtained by QM/MM umbrella sampling simulations. A schematic representation of the QM subsystem and the reaction coordinate (ξ) definition are shown.

substrate positioning and thus its interactions with different chemical groups of the enzyme, we decided to determine the overoxidation reaction free energy profile starting from a representative structure of each one, in order to evaluate the consequences of these dynamical characteristics on the reactivity properties of the system.

3.2. Reactions Evolution and Mechanism. The free energy profiles and the corresponding free energy barriers ($\Delta G^{\dagger}$) of the studied reactions are shown in Figure 4B and Table 2. Free energy barriers of these reactions are sensitive to the level of theory used and/or to the presence of explicit water molecules in the simulated system, as has been discussed previously.[27] Except for an earlier transition state (TS) found for the reaction of $MeSO^-$ in aqueous solution with respect to the Cys_P-SO^- in the enzyme (ξ values of −0.9 and −0.7 Å, respectively), no significant changes were observed regarding the operative reaction mechanism: in both enzyme and solution environments, the overoxidation reaction could be described as a bimolecular nucleophilic substitution followed by a proton transfer. Three major processes were observed to describe the evolution of the reaction: the S−O_R bond formation, the O_R−O_W bond breaking, and the proton transfer from O_R to O_W to yield a water molecule. This mechanistic behavior showed analogies with that of the oxidation of thiolates.[4,42,61,78,79] Since the proton is transferred after the TS is reached, the selection of the reaction coordinate is expected to have reliable free activation energies, and the reaction free energies might be even lower (more negative) than the ones reported in this work, for which the direct calculation of an equilibrium constant or a redox potential might be prone to large errors. Nevertheless, all the reactions under investigation turn out to be strongly exergonic (being completely irreversible), and errors coming from the lack of sampling of the hydrogen transfer process or from Hamiltonian flaws would not affect the overall trend (Figure 4B).

Table 2. Free Energy Barriers for $MeSO^-$ and *Mt*AhpE-Cys_P-SO^- Reactions with H_2O_2 Obtained by Electronic Structure Calculations or by QM/MM Umbrella Sampling Simulations

reaction	method	$\Delta G^{\dagger}$ (kcal/mol)
$MeSO^- + H_2O_2 \rightarrow MeSO_2^- + H_2O$	in vacuo/PBE/dzvp	12
	in vacuo/MP2/dzvp	24
	QM/MM/PBE/dzvp umbrella sampling	9.6 ± 0.7
Cys_P-$SO^- + H_2O_2 \rightarrow Cys_P$-$SO_2^- + H_2O$ (conformation II)	QM/MM/PBE/dzvp umbrella sampling	16.0 ± 0.5

The $\Delta G^{\dagger}$ values (Figure 4B) show that the enzyme microenvironment raises the value of the barrier by ∼3−6 kcal/mol (depending on the starting conformation) compared to the reaction in aqueous solution, which suggests that residues and interactions that are responsible for the oxidation catalysis do not play a catalytic role in the overoxidation reaction.[61] Additionally, the comparison of the results obtained in vacuo for $MeSO^-$, by means of electronic structure calculations, and those coming from the QM/MM MD shows that the aqueous solvent lowers the barrier and that the PBE functional underestimates the free energy barrier in comparison with the MP2 method, which could be possibly attributed to the flaws of DFT at the GGA level for describing transition states.[65,80] The TS structures obtained in vacuo (which were confirmed through IRC calculations) and from the QM/MM simulations were very similar, supporting the reliability of these results.

Given the exponential dependence of the rate constant on the free energy barrier (due to Eyring's equation[81]), even small errors on the latter would lead to large variations in the calculated rate constant, and as shown in Table 2, the electronic structure method strongly affects the absolute value of the computed barriers. However, the ratio between the rate constants of two bimolecular reactions (namely, k_1 and k_2) can be roughly estimated as $k_1/k_2 = \exp(\Delta G_2^{\dagger} - \Delta G_1^{\dagger})$, assuming compensation of errors in the computed barriers. From the free energy profiles shown in Figure 4, Cys_P-SO^- in conformations I and II (Figure 4) is expected to react ∼10^4 times slower than $MeSO^-$, while a ∼10^2 factor is expected for conformation III. Additionally, the obtained $\Delta G^{\dagger}$ values for the *Mt*AhpE overoxidation are several kilocalories per mole lower

DOI: 10.1021/acs.jcim.9b00817
J. Chem. Inf. Model. XXXX, XXX, XXX−XXX

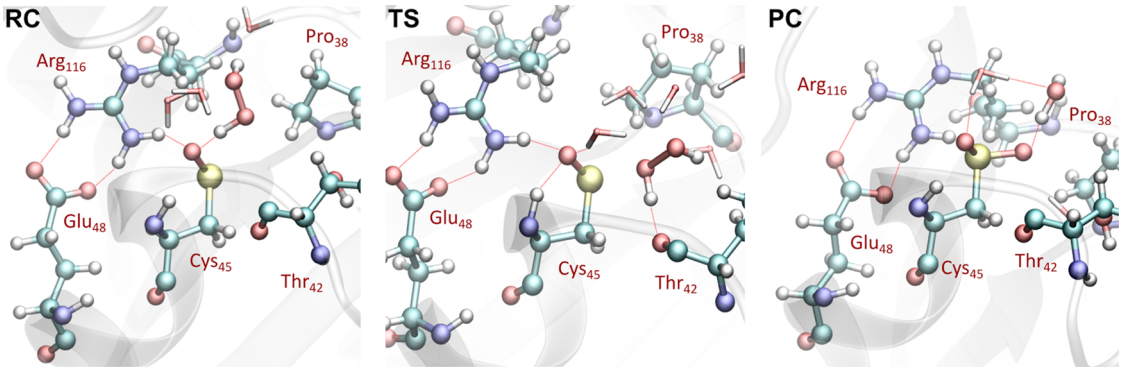

Figure 5. Representative snapshots of reactant complex (RC), transition state (TS), and product complex (PC) for the oxidation of Cys_P-SO^- (conformation II) by H_2O_2, obtained by umbrella sampling QM/MM simulations.

than the experimentally determined 10.5 kcal/mol for the oxidation process,[61] and the same trend is observed when comparing with computationally estimated barriers.[4,61] These results are in qualitative agreement with the lower second-order rate constants determined for this reaction in several enzymes (Table 1) in comparison to those of the oxidation process (the oxidation being ~10^3 faster at 25 °C in the particular case of *Mt*AhpE).[12,22,41,61]

On the other hand, the oxidation reaction has been reported to be accelerated ~10^4 times by the enzyme, which in turn emphasizes the unfavorable microenvironment that the enzyme provides for the overoxidation reaction in contrast with the oxidation reaction (in each case, relative to the corresponding reaction in aqueous solution). In our previous study of the oxidation reaction, the exploration of the free energy landscape using the umbrella sampling method allowed us to identify key events during the oxidation reaction, and the obtained $\Delta\Delta G^{\ddagger}$ of ~4 kcal/mol was in reasonable agreement with the 4 orders of magnitude increase in the oxidation rate constants and the experimental $\Delta\Delta G^{\ddagger}$ of 5.4 kcal/mol.[61] Furthermore, the strong interactions of the thiolate and the peroxide with Arg116 and Thr42 residues, which are extremely conserved among the Prx family, confirmed that these are key residues in the stabilization of the TS due to an active site design that sets up a complex H-bond network. This is consistent with the decrease of reactivity with hydrogen peroxide previously measured for *Mt*AhpE variants lacking these residues.[82] More precisely, Arg116, which is initially oriented to the thiolate with both N atoms equidistant to the S atom (see Figure 3D), turns toward one of the O atoms of the peroxide facilitating the TS linear arrangement and its stabilization through H-bond interactions involving also the Thr42 hydroxyl group. However, when the sulfenate is formed, Arg116 interacts through two H-bonds with Glu48 in conformations I and II (Figure 3E). In conformation III, Arg116 is oriented outward from the active site and interacts with Glu48, forming only one H-bond. The presence of this double H-bond interaction in conformations I and II leads to a different behavior of the Arg116 that practically does not change its orientation or distance with Cys_P (Cys45 in Figure 5 and Supporting Information Figure S4) through the reaction. Only conformation III exhibits some mobility in Arg116 but always maintains its position far from the active site.

Taking into account that the TS structure turned out to be qualitatively the same for the three conformations studied and for the reaction in solution, we further investigate if the differences in the free energy barriers could be related not to significant changes in the TS structure but to the differential stabilization of the RC and TS in each case.

3.3. Charges Distribution and Solvation Patterns Evolution. Regarding nucleophilic substitutions, free energy barriers can be interpreted in terms of charges redistribution since the reaction is driven by the tendency of the electrophile to become more negative. In this work, we monitored the charge redistribution by means of Mulliken's populations over relevant atoms along the reaction, by computing the average values for each umbrella sampling window (see Figures 6 and

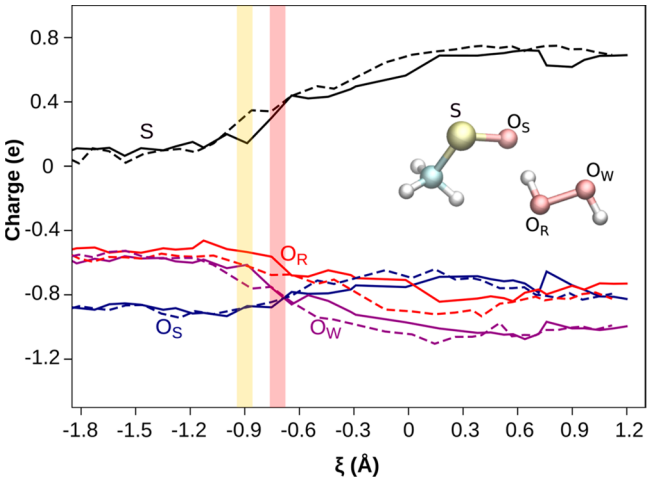

Figure 6. Mulliken charge evolution for the reaction of H_2O_2 with $MeSO^-$ and *Mt*AhpE-Cys_P-SO^- in conformation II (dashed and solid lines, respectively). The reaction coordinate values corresponding to the TS regions are indicated by a yellow and a red box for the reaction in aqueous solution and protein, respectively. Labels are shown on a representative snapshot of the QM subsystem.

Supporting Information Figure S5). In general, evolution of charges is quite similar between the reaction in solution and in the enzymatic environment, being practically identical among the three conformations. At the same time that the S atom becomes more positive, its charge is transferred to both O_R and O_W atoms of hydrogen peroxide. The O_S atom's charge, on the other hand, remains almost unmodified from the RC to the TS. In the oxidation reaction, the enzyme provides a set of interactions described above which carefully guides this process, allowing the charge redistribution to take place at a lower energy cost compared to the reaction in aqueous solution. The opposite effect is observed in the overoxidation

DOI: 10.1021/acs.jcim.9b00817
J. Chem. Inf. Model. XXXX, XXX, XXX−XXX

process, where the amount of charge transferred at around −0.9 Å of the reaction coordinate (corresponding to TS for the reaction in solution, yellow box in Figure 6) is lower than that of the enzyme, at the same reaction coordinate value. In other words, at the same stage of the reaction, the S atom is more positive, and O_R and O_W are more negative in the reaction in solution than in the enzyme. Interestingly, in the enzyme, once the TS is reached, charges coincide approximately to those of the TS in solution, which suggests that the free energy reaches its maximum only once a certain amount of charge gets distributed. The charge transfer from the nucleophilic center (the S atom) to the hydroperoxide is achieved more easily (at an earlier reaction coordinate value and with a lower free energy cost) in aqueous solution than in this enzyme microenvironment.

An interesting issue is how water molecules facilitate the charge distribution needed in order to reach the TS and so overcome the reaction free energy barrier. With the aim of answering this question, we computed radial correlation functions ($g(r)$) centered in selected atoms with respect to oxygen water molecules at different stages of the reaction (see Figures 7 and Supporting Information Figure S3). Typically, the first solvation shell (given by the first peak of the radial correlation function) is centered between ∼2.7 and 3.0 Å (radial distance) for oxygen atoms, while the S atom practically lacks a solvation structure. More importantly, both in enzyme reactions and in solution reactions, the O_S atom is pointing to the O_R atom from the hydroperoxide at RC, while in the TS an O_S-S-O_R angle is slightly larger than 90° (see Figures 5 and 7), allowing the O_S atom to be fully solvated. Therefore, even though the charge on the O_S atom does not change significantly from RC to TS, it becomes significantly more solvated at the TS, as reflected in the increase of the O_S $g(r)$ first peak for the reaction in solution (Figure 7).

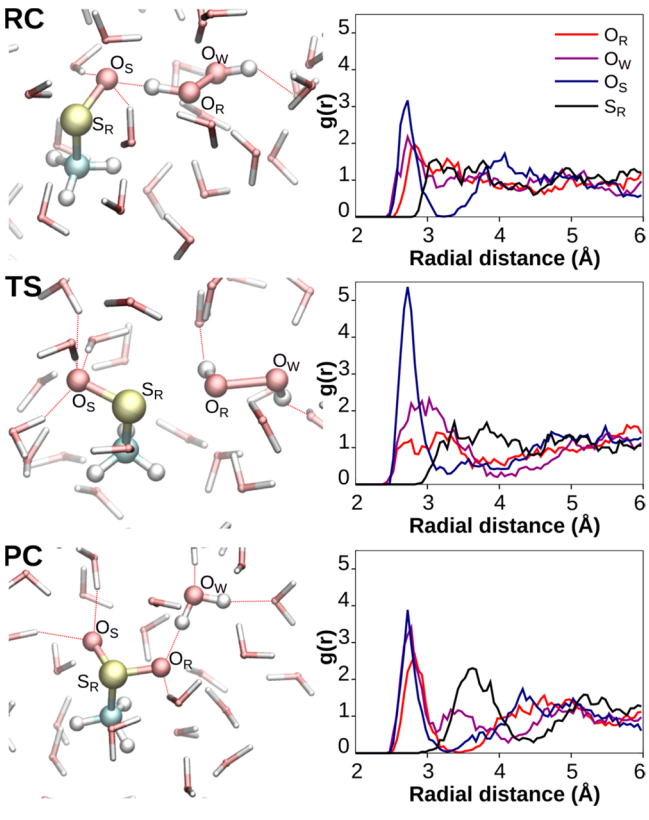

Figure 7. Left: Representative snapshots of reactant complex (RC), transition state (TS), and product complex (PC) for the oxidation of $MeSO^-$ by H_2O_2 in aqueous solution, obtained by umbrella sampling QM/MM simulation. Bond interactions within centers closer than 2 Å are depicted. Right: Corresponding radial correlation functions for selected atoms with respect to MM water oxygen atoms obtained by performing 50 ps QM/MM sampling with the stochastic Langevin thermostat model.

In the enzymatic environment, other residues, like Arg116 (conformation I and II, Figure 4), interact with O_S at the TS, replacing the solvent molecules, and solvation patterns remain almost unaffected from RC to TS (see Supporting Information Figure S3). The only exception is conformation III, in which the different orientation of Arg116 allows the entrance of more water molecules into the active site, and particularly the O_W atom becomes more solvated at the TS. These differences in solvation patterns between RC and TS account for the observed tendency in the free energy profiles: the more efficiently the TS is solvated, compared to the RC, the lower the free energy barrier. Finally, these results also suggest that there is no specific stabilization of the RC or TS provided by residues of the active site, since the differential solvation rationale seems to account for all the observed differences between the free energy barriers of the reaction in solution and in the enzyme and between the three enzyme conformations studied.

4. CONCLUSIONS

A multiscale study of the H_2O_2-mediated oxidation of sulfenates either in a LMW compound as well as in a peroxidatic cysteine residue was performed. *Mt*AhpE-Cys_p-SO^- and $MeSO^-$ were selected as examples and free energy profiles calculations by means of the umbrella sampling method, which allowed us to estimate free energy barriers as well as mechanistic information and evolution of key properties through the process for each case.

In the case of *Mt*AhpE-Cys_p-SO^-, we analyzed and compared three different starting conformations obtained by relatively long classical simulations of the enzyme with a H_2O_2 molecule restrained close to its active site. These conformations differed mainly on the orientation of H_2O_2 and Arg116, a strictly conserved residue in this enzyme family and actively contributing in the oxidation step of the catalytic cycle. The different interaction network at the active site was useful for understanding the influence of certain residues and solvent molecules in the free energy barriers obtained. In comparison with the reaction in solution, our results suggest that the *Mt*AhpE environment does not accelerate the overoxidation process by hydrogen peroxide. The possible role of protein microenvironment in overoxidation caused by other hydroperoxides such as fatty acid hydroperoxides, that are not only highly efficient substrates for this enzyme but also rapidly inactivate it through overoxidation,[29,42] should be a matter of further investigation. Moreover, the free energy barriers showed that overoxidation is unfavored by the enzyme, which can be related to a better stabilization of the TS in aqueous solution because of a significant increase in the local solvation of O_S with respect to the RC stage. In this context, the advantages of the QM/MM approach, which allowed us to explore the free energy landscape including explicitly the solvent water molecules at an affordable cost, are highlighted. Finally, free energy profiles allowed us to obtain not only mechanistic information but also kinetic and thermodynamic

DOI: 10.1021/acs.jcim.9b00817
J. Chem. Inf. Model. XXXX, XXX, XXX−XXX

properties that could be directly compared with experimental data for validating the methodology. In addition, we have shown that properties such as the evolution of charge distribution, solvation patterns, and geometric parameters that cannot be easily assessed experimentally can be estimated quite directly from the simulations and offer useful information for the understanding of the reactive processes in complex environments.

■ ASSOCIATED CONTENT

Supporting Information

The Supporting Information is available free of charge at https://pubs.acs.org/doi/10.1021/acs.jcim.9b00817.

Figures S1−S5 (PDF)

■ AUTHOR INFORMATION

Corresponding Authors

*E-mail: azeida@fmed.edu.uy.

*E-mail: dario@qi.fcen.uba.ar.

ORCID

R. Radi: 0000-0002-1114-1875

D. A. Estrin: 0000-0002-5006-7225

Notes

The authors declare no competing financial interest.

■ ACKNOWLEDGMENTS

J.S. is supported by doctoral fellowship from Consejo Nacional de Investigaciones Científicas y Técnicas (CONICET). J.S. and D.A.E. gratefully acknowledge the funding from Universidad de Buenos Aires (UBACYT 20020130100097BA) and Agencia Nacional de Promoción Científica y Tecnológica (PICT 2014-1022, and PICT 2015-2761) and CONICET Grant 11220150100303CO. F.B. was supported by a Santander Ibero-America grant. A.Z. is supported by a posdoctoral fellowship from Agencia Nacional de Investigación e Innovación (ANII), Uruguay. R.R., M.T., and A.Z. are grateful for funding from Comisión Sectorial de Investigación Científica (CSIC I+D 2016 to M.T. and CSIC Grupos 2018 to R.R.); Espacio Interdisciplinario (Centros_2015 to R.R.); Universidad de la República, Ministerio de Educación y Cultura (Fondo Vaz Ferreira 2018 to A.Z.), Uruguay; Centro de Biología Estructural Mercosur (CeBEM); Centro de Computación de Alto Rendimiento (CeCAR) de la Facultad de Ciencias Exactas y Naturales de la UBA; and Programa de Desarrollo de Ciencias Básicas (PEDECIBA), Uruguay.

■ REFERENCES

(1) Crespo, A.; Scherlis, D. A.; Martí, M. A.; Ordejón, P.; Roitberg, A. E.; Estrin, D. A. A DFT-Based QM-MM Approach Designed for the Treatment of Large Molecular Systems: Application to Chorismate Mutase. *J. Phys. Chem. B* **2003**, *107*, 13728−13736.

(2) Crespo, A.; Martí, M. A.; Kalko, S. G.; Morreale, A.; Orozco, M.; Gelpi, J. L.; Luque, F. J.; Estrin, D. A. Theoretical Study of the Truncated Hemoglobin HbN: Exploring the Molecular Basis of the NO Detoxification Mechanism. *J. Am. Chem. Soc.* **2005**, *127*, 4433−4444.

(3) Lewis-Ballester, A.; Batabyal, D.; Egawa, T.; Lu, C.; Lin, Y.; Marti, M. A.; Capece, L.; Estrin, D. A.; Yeh, S.-R. Evidence for a Ferryl Intermediate in a Heme-Based Dioxygenase. *Proc. Natl. Acad. Sci. U. S. A.* **2009**, *106*, 17371−17376.

(4) Marcolongo, J. P.; Zeida, A.; Semelak, J. A.; Foglia, N. O.; Morzan, U. N.; Estrin, D. A.; González Lebrero, M. C.; Scherlis, D. A. Chemical Reactivity and Spectroscopy Explored From QM/MM Molecular Dynamics Simulations Using the LIO Code. *Front. Chem.* **2018**, *6*, DOI: 10.3389/fchem.2018.00070.

(5) Nitsche, M. A.; Ferreria, M.; Mocskos, E. E.; González Lebrero, M. C. GPU Accelerated Implementation of Density Functional Theory for Hybrid QM/MM Simulations. *J. Chem. Theory Comput.* **2014**, *10*, 959−967.

(6) Joseph, C. A.; Maroney, M. J. Cysteine Dioxygenase: Structure and Mechanism. *Chem. Commun.* **2007**, 3338−3349.

(7) Akter, S.; Fu, L.; Jung, Y.; Conte, M. L.; Lawson, J. R.; Lowther, W. T.; Sun, R.; Liu, K.; Yang, J.; Carroll, K. S. Chemical Proteomics Reveals New Targets of Cysteine Sulfinic Acid Reductase. *Nat. Chem. Biol.* **2018**, *14*, 995−1004.

(8) Lee, C.-F.; Paull, T. T.; Person, M. D. Proteome-Wide Detection and Quantitative Analysis of Irreversible Cysteine Oxidation Using Long Column UPLC-PSRM. *J. Proteome Res.* **2013**, *12*, 4302−4315.

(9) Hamann, M.; Zhang, T.; Hendrich, S.; Thomas, J. A. [15] Quantitation of Protein Sulfinic and Sulfonic Acid, Irreversibly Oxidized Protein Cysteine Sites in Cellular Proteins. In *Methods in Enzymology*; Elsevier, 2002; Vol. *348*, pp 146−156.

(10) Jacob, C.; Holme, A. L.; Fry, F. H. The Sulfinic Acid Switch in Proteins. *Org. Biomol. Chem.* **2004**, *2*, 1953−1956.

(11) Yang, K.-S.; Kang, S. W.; Woo, H. A.; Hwang, S. C.; Chae, H. Z.; Kim, K.; Rhee, S. G. Inactivation of Human Peroxiredoxin I during Catalysis as the Result of the Oxidation of the Catalytic Site Cysteine to Cysteine-Sulfinic Acid. *J. Biol. Chem.* **2002**, *277*, 38029−38036.

(12) Trujillo, M.; Alvarez, B.; Radi, R. One-and Two-Electron Oxidation of Thiols: Mechanisms, Kinetics and Biological Fates. *Free Radical Res.* **2016**, *50*, 150−171.

(13) Sevilla, M.; Becker, D.; Yan, M. The Formation and Structure of the Sulfoxyl Radicals RSO·, RSOO·, RSO_2·, and RSO_2OO· from the Reaction of Cysteine, Glutathione and Penicillamine Thiyl Radicals with Molecular Oxygen. *Int. J. Radiat. Biol.* **1990**, *57*, 65−81.

(14) Xu, G.; Chance, M. R. Radiolytic Modification of Sulfur-Containing Amino Acid Residues in Model Peptides: Fundamental Studies for Protein Footprinting. *Anal. Chem.* **2005**, *77*, 2437−2449.

(15) Winterbourn, C. C. Biological Production, Detection, and Fate of Hydrogen Peroxide. *Antioxid. Redox Signaling* **2018**, *29*, 541−551.

(16) Rhee, S. G. A Catalytic Career: Studies Spanning Glutamine Synthetase, Phospholipase C, Peroxiredoxin, and the Intracellular Messenger Role of Hydrogen Peroxide. *J. Biol. Chem.* **2019**, *294*, 5169−5180.

(17) Winterbourn, C. C.; Metodiewa, D. Reactivity of Biologically Important Thiol Compounds with Superoxide and Hydrogen Peroxide. *Free Radical Biol. Med.* **1999**, *27*, 322−328.

(18) Portillo-Ledesma, S.; Sardi, F.; Manta, B.; Tourn, M. V.; Clippe, A.; Knoops, B.; Alvarez, B.; Coitiño, E. L.; Ferrer-Sueta, G. Deconstructing the Catalytic Efficiency of Peroxiredoxin-5 Peroxidatic Cysteine. *Biochemistry* **2014**, *53*, 6113−6125.

(19) Poole, L. The Catalytic Mechanism of Peroxiredoxins. In *Peroxiredoxin Systems*; Flohé, L., Harris, J. R., Eds.; Subcellular Biochemistry, Springer, New York, 2007.

(20) Perkins, A.; Nelson, K. J.; Parsonage, D.; Poole, L. B.; Karplus, P. A. Peroxiredoxins: Guardians against Oxidative Stress and Modulators of Peroxide Signaling. *Trends Biochem. Sci.* **2015**, *40*, 435−445.

(21) Flohé, L.; Toppo, S.; Cozza, G.; Ursini, F. A Comparison of Thiol Peroxidase Mechanisms. *Antioxid. Redox Signaling* **2011**, *15*, 763−780.

(22) Zeida, A.; Trujillo, M.; Ferrer-Sueta, G.; Denicola, A.; Estrin, D. A.; Radi, R. Catalysis of Peroxide Reduction by Fast Reacting Protein Thiols. *Chem. Rev.* **2019**, *119*, 10829.

(23) Lo Conte, M.; Carroll, K. S. The Redox Biochemistry of Protein Sulfenylation and Sulfinylation. *J. Biol. Chem.* **2013**, *288*, 26480−26488.

(24) Abedinzadeh, Z.; Gardes-Albert, M.; Ferradini, C. Kinetic study of the oxidation mechanism of glutathione by hydrogen peroxide in neutral aqueous medium. *Can. J. Chem.* **1989**, *67*, 1247−1255.

DOI: 10.1021/acs.jcim.9b00817
J. Chem. Inf. Model. XXXX, XXX, XXX−XXX

(25) Chauvin, J.-P. R.; Pratt, D. A. On the Reactions of Thiols, Sulfenic Acids, and Sulfinic Acids with Hydrogen Peroxide. *Angew. Chem., Int. Ed.* **2017**, *56* (22), 6255−6259.
(26) Hugo, M.; Turell, L.; Manta, B.; Botti, H.; Monteiro, G.; Netto, L. E.; Alvarez, B.; Radi, R.; Trujillo, M. Thiol and Sulfenic Acid Oxidation of AhpE, the One-Cysteine Peroxiredoxin from Mycobacterium Tuberculosis: Kinetics, Acidity Constants, and Conformational Dynamics. *Biochemistry* **2009**, *48*, 9416−9426.
(27) van Bergen, L. A.; Roos, G.; De Proft, F. From Thiol to Sulfonic Acid: Modeling the Oxidation Pathway of Protein Thiols by Hydrogen Peroxide. *J. Phys. Chem. A* **2014**, *118*, 6078−6084.
(28) Rabilloud, T.; Heller, M.; Gasnier, F.; Luche, S.; Rey, C.; Aebersold, R.; Benahmed, M.; Louisot, P.; Lunardi, J. Proteomics Analysis of Cellular Response to Oxidative Stress Evidence for in Vivo Overoxidation of Peroxiredoxins at Their Active Site. *J. Biol. Chem.* **2002**, *277*, 19396−19401.
(29) Reyes, A. M.; Hugo, M.; Trostchansky, A.; Capece, L.; Radi, R.; Trujillo, M. Oxidizing Substrate Specificity of Mycobacterium Tuberculosis Alkyl Hydroperoxide Reductase E: Kinetics and Mechanisms of Oxidation and Overoxidation. *Free Radical Biol. Med.* **2011**, *51*, 464−473.
(30) Peskin, A. V.; Dickerhof, N.; Poynton, R. A.; Paton, L. N.; Pace, P. E.; Hampton, M. B.; Winterbourn, C. C. Hyperoxidation of Peroxiredoxins 2 and 3: Rate Constants for the Reactions of the Sulfenic Acid of the Peroxidatic Cysteine. *J. Biol. Chem.* **2013**, *288*, 14170−14177.
(31) Karplus, P. A. A Primer on Peroxiredoxin Biochemistry. *Free Radical Biol. Med.* **2015**, *80*, 183−190.
(32) Wood, Z. A.; Poole, L. B.; Karplus, P. A. Peroxiredoxin Evolution and the Regulation of Hydrogen Peroxide Signaling. *Science* **2003**, *300*, 650−653.
(33) Song, I.-K.; Lee, J.-J.; Cho, J.-H.; Jeong, J.; Shin, D.-H.; Lee, K.-J. Degradation of Redox-Sensitive Proteins Including Peroxiredoxins and DJ-1 Is Promoted by Oxidation-Induced Conformational Changes and Ubiquitination. *Sci. Rep.* **2016**, *6*, 34432.
(34) Chang, T.-S.; Jeong, W.; Woo, H. A.; Lee, S. M.; Park, S.; Rhee, S. G. Characterization of Mammalian Sulfiredoxin and Its Reactivation of Hyperoxidized Peroxiredoxin through Reduction of Cysteine Sulfinic Acid in the Active Site to Cysteine. *J. Biol. Chem.* **2004**, *279*, 50994−51001.
(35) Nelson, K. J.; Perkins, A.; Van Swearingen, A. E. D.; Hartman, S.; Brereton, A. E.; Parsonage, D.; Salsbury, F. R.; Karplus, P. A.; Poole, L. B. Experimentally Dissecting the Origins of Peroxiredoxin Catalysis. *Antioxid. Redox Signaling* **2018**, *28*, 521−536.
(36) Salsbury, F. R.; Yuan, Y.; Knaggs, M. H.; Poole, L. B.; Fetrow, J. S. Structural and Electrostatic Asymmetry at the Active Site in Typical and Atypical Peroxiredoxin Dimers. *J. Phys. Chem. B* **2012**, *116*, 6832−6843.
(37) Yuan, Y.; Knaggs, M. H.; Poole, L. B.; Fetrow, J. S.; Salsbury, F. R. Conformational and Oligomeric Effects on the Cysteine PK(a) of Tryparedoxin Peroxidase. *J. Biomol. Struct. Dyn.* **2010**, *28*, 51−70.
(38) Wang, X.; Wang, L.; Wang, X.; Sun, F.; Wang, C. Structural Insights into the Peroxidase Activity and Inactivation of Human Peroxiredoxin 4. *Biochem. J.* **2012**, *441*, 113−118.
(39) Randall, L.; Manta, B.; Nelson, K. J.; Santos, J.; Poole, L. B.; Denicola, A. Structural Changes upon Peroxynitrite-Mediated Nitration of Peroxiredoxin 2; Nitrated Prx2 Resembles Its Disulfide-Oxidized Form. *Arch. Biochem. Biophys.* **2016**, *590*, 101−108.
(40) Noichri, Y.; Palais, G.; Ruby, V.; D'Autreaux, B.; Delaunay-Moisan, A.; Nyström, T.; Molin, M.; Toledano, M. B. In Vivo Parameters Influencing 2-Cys Prx Oligomerization: The Role of Enzyme Sulfinylation. *Redox Biol.* **2015**, *6*, 326−333.
(41) Hugo, M.; Van Laer, K.; Reyes, A. M.; Vertommen, D.; Messens, J.; Radi, R.; Trujillo, M. Mycothiol/Mycoredoxin 1-Dependent Reduction of the Peroxiredoxin AhpE from Mycobacterium Tuberculosis. *J. Biol. Chem.* **2014**, *289*, 5228−5239.
(42) Zeida, A.; Reyes, A. M.; Lichtig, P.; Hugo, M.; Vazquez, D. S.; Santos, J.; González Flecha, F. L.; Radi, R.; Estrin, D. A.; Trujillo, M. Molecular Basis of Hydroperoxide Specificity in Peroxiredoxins: The Case of AhpE from Mycobacterium Tuberculosis. *Biochemistry* **2015**, *54*, 7237−7247.
(43) Cuevasanta, E.; Reyes, A. M.; Zeida, A.; Mastrogiovanni, M.; De Armas, M. I.; Radi, R.; Alvarez, B.; Trujillo, M. Kinetics of Formation and Reactivity of the Persulfide in the One-Cysteine Peroxiredoxin from Mycobacterium Tuberculosis. *J. Biol. Chem.* **2019**, *294*, 13593.
(44) Dalla Rizza, J.; Randall, L. M.; Santos, J.; Ferrer-Sueta, G.; Denicola, A. Differential Parameters between Cytosolic 2-Cys Peroxiredoxins, PRDX1 and PRDX2. *Protein Sci.* **2019**, *28*, 191−201.
(45) Stone, J. R. An Assessment of Proposed Mechanisms for Sensing Hydrogen Peroxide in Mammalian Systems. *Arch. Biochem. Biophys.* **2004**, *422*, 119−124.
(46) Peskin, A. V.; Pace, P. E.; Winterbourn, C. C. Enhanced Hyperoxidation of Peroxiredoxin 2 and Peroxiredoxin 3 in the Presence of Bicarbonate/CO2. *Free Radical Biol. Med.* **2019**, *145*, 1.
(47) De Armas, M. I.; Esteves, R.; Viera, N.; Reyes, A. M.; Mastrogiovanni, M.; Alegria, T. G. P.; Netto, L. E. S.; Tórtora, V.; Radi, R.; Trujillo, M. Rapid Peroxynitrite Reduction by Human Peroxiredoxin 3: Implications for the Fate of Oxidants in Mitochondria. *Free Radical Biol. Med.* **2019**, *130*, 369−378.
(48) Alvarez, B.; Carballal, S.; Turell, L.; Radi, R. Chapter 5 - Formation and Reactions of Sulfenic Acid in Human Serum Albumin. In *Methods in Enzymology*; Cadenas, E., Packer, L., Eds.; Thiol Redox Transitions in Cell Signaling, Part A: Chemistry and Biochemistry of Low Molecular Weight and Protein Thiols, Academic Press, 2010; Vol. *473*, pp 117−136.
(49) Sohn, J.; Rudolph, J. Catalytic and Chemical Competence of Regulation of Cdc25 Phosphatase by Oxidation/Reduction. *Biochemistry* **2003**, *42*, 10060−10070.
(50) Poole, L. B.; Claiborne, A. The Non-Flavin Redox Center of the Streptococcal NADH Peroxidase. II. Evidence for a Stabilized Cysteine-Sulfenic Acid. *J. Biol. Chem.* **1989**, *264*, 12330−12338.
(51) Crane, E. J.; Parsonage, D.; Claiborne, A. The Active-Site Histidine-10 of Enterococcal NADH Peroxidase Is Not Essential for Catalytic Activity. *Biochemistry* **1996**, *35*, 2380.
(52) Li, S.; Peterson, N. A.; Kim, M.-Y.; Kim, C.-Y.; Hung, L.-W.; Yu, M.; Lekin, T.; Segelke, B. W.; Lott, J. S.; Baker, E. N. Crystal Structure of AhpE from Mycobacterium Tuberculosis, a 1-Cys Peroxiredoxin. *J. Mol. Biol.* **2005**, *346*, 1035−1046.
(53) van Bergen, L. A. H.; Alonso, M.; Palló, A.; Nilsson, L.; De Proft, F.; Messens, J. Revisiting Sulfur H-Bonds in Proteins: The Example of Peroxiredoxin AhpE. *Sci. Rep.* **2016**, *6*, 30369.
(54) Jorgensen, W. L.; Chandrasekhar, J.; Madura, J. D.; Impey, R. W.; Klein, M. L. Comparison of Simple Potential Functions for Simulating Liquid Water. *J. Chem. Phys.* **1983**, *79*, 926−935.
(55) Maier, J. A.; Martinez, C.; Kasavajhala, K.; Wickstrom, L.; Hauser, K. E.; Simmerling, C. Ff14SB: Improving the Accuracy of Protein Side Chain and Backbone Parameters from Ff99SB. *J. Chem. Theory Comput.* **2015**, *11*, 3696−3713.
(56) Wang, J.; Wolf, R. M.; Caldwell, J. W.; Kollman, P. A.; Case, D. A. Development and Testing of a General Amber Force Field. *J. Comput. Chem.* **2004**, *25*, 1157−1174.
(57) Ryckaert, J.-P.; Ciccotti, G.; Berendsen, H. J. C. Numerical Integration of the Cartesian Equations of Motion of a System with Constraints: Molecular Dynamics of n-Alkanes. *J. Comput. Phys.* **1977**, *23*, 327−341.
(58) Schneider, T.; Stoll, E. Molecular-Dynamics Study of a Three-Dimensional One-Component Model for Distortive Phase Transitions. *Phys. Rev. B: Condens. Matter Mater. Phys.* **1978**, *17*, 1302−1322.
(59) Feller, S. E.; Zhang, Y.; Pastor, R. W.; Brooks, B. R. Constant Pressure Molecular Dynamics Simulation: The Langevin Piston Method. *J. Chem. Phys.* **1995**, *103*, 4613−4621.
(60) Berendsen, H. J.; Postma, J. P. M.; van Gunsteren, W. F.; DiNola, A.; Haak, J. Molecular Dynamics with Coupling to an External Bath. *J. Chem. Phys.* **1984**, *81*, 3684−3690.
(61) Zeida, A.; Reyes, A. M.; Lebrero, M. C. G.; Radi, R.; Trujillo, M.; Estrin, D. A. The Extraordinary Catalytic Ability of Peroxiredox-

DOI: 10.1021/acs.jcim.9b00817
J. Chem. Inf. Model. XXXX, XXX, XXX−XXX

ins: A Combined Experimental and QM/MM Study on the Fast Thiol Oxidation Step. *Chem. Commun.* **2014**, *50*, 10070−10073.
(62) Frisch, M.; Trucks, G.; Schlegel, H.; Scuseria, G.; Robb, M.; Cheeseman, J.; Scalmani, G.; Barone, V.; Mennucci, B.; Petersson, G. *Gaussian 09*; Gaussian Inc.: Wallingford, CT, 2009.
(63) Godbout, N.; Salahub, D. R.; Andzelm, J.; Wimmer, E. Optimization of Gaussian-Type Basis Sets for Local Spin Density Functional Calculations. Part I. Boron through Neon, Optimization Technique and Validation. *Can. J. Chem.* **1992**, *70*, 560−571.
(64) Fukui, K. The path of chemical reactions-the IRC approach. *Acc. Chem. Res.* **1981**, *14*, 363−368.
(65) Neves, R. P.; Fernandes, P. A.; Varandas, A. J.; Ramos, M. J. Benchmarking of Density Functionals for the Accurate Description of Thiol−Disulfide Exchange. *J. Chem. Theory Comput.* **2014**, *10*, 4842−4856.
(66) Nitsche, M. A.; Ferreria, M.; Mocskos, E. E.; Gonzalez Lebrero, M. C. GPU Accelerated Implementation of Density Functional Theory for Hybrid QM/MM Simulations. *J. Chem. Theory Comput.* **2014**, *10*, 959−967.
(67) Humphrey, W.; Dalke, A.; Schulten, K. VMD: Visual Molecular Dynamics. *J. Mol. Graphics* **1996**, *14*, 33−38.
(68) Kumar, S.; Rosenberg, J. M.; Bouzida, D.; Swendsen, R. H.; Kollman, P. A. The Weighted Histogram Analysis Method for Free-Energy Calculations on Biomolecules. I. The Method. *J. Comput. Chem.* **1992**, *13*, 1011−1021.
(69) Kastner, J. Umbrella Sampling. *Wiley Interdiscip. Rev. Comput. Mol. Sci.* **2011**, *1*, 932−942.
(70) Branduardi, D.; Gervasio, F. L.; Parrinello, M. From A to B in Free Energy Space. *J. Chem. Phys.* **2007**, *126*, 054103.
(71) Peters, B.; Beckham, G. T.; Trout, B. L. Extensions to the Likelihood Maximization Approach for Finding Reaction Coordinates. *J. Chem. Phys.* **2007**, *127*, 034109.
(72) Quapp, W. Chemical Reaction Paths and Calculus of Variations. *Theor. Chem. Acc.* **2008**, *121*, 227−237.
(73) Rosta, E.; Woodcock, H. L.; Brooks, B. R.; Hummer, G. Artificial Reaction Coordinate "Tunneling" in Free-Energy Calculations: The Catalytic Reaction of RNase H. *J. Comput. Chem.* **2009**, *30*, 1634−1641.
(74) Kastner, J.; Thiel, W. Bridging the Gap between Thermodynamic Integration and Umbrella Sampling Provides a Novel Analysis Method:"Umbrella Integration. *J. Chem. Phys.* **2005**, *123*, 144104.
(75) Kumar, A.; Balakrishna, A. M.; Nartey, W.; Manimekalai, M. S. S.; Grüber, G. Redox Chemistry of Mycobacterium Tuberculosis Alkylhydroperoxide Reductase E (AhpE): Structural and Mechanistic Insight into a Mycoredoxin-1 Independent Reductive Pathway of AhpE via Mycothiol. *Free Radical Biol. Med.* **2016**, *97*, 588−601.
(76) Salsbury, F. R., Jr; Knutson, S. T.; Poole, L. B.; Fetrow, J. S. Functional site profiling and electrostatic analysis of cysteines modifiable to cysteine sulfenic acid. *Protein Sci.* **2008**, *17*, 299−312.
(77) Perkins, A.; Parsonage, D.; Nelson, K. J.; Ogba, O. M.; Cheong, P. H.-Y.; Poole, L. B.; Karplus, P. A. Peroxiredoxin Catalysis at Atomic Resolution. *Structure* **2016**, *24*, 1668−1678.
(78) Zeida, A.; Gonzalez Lebrero, M. C.; Radi, R.; Trujillo, M.; Estrin, D. A. Mechanism of Cysteine Oxidation by Peroxynitrite: An Integrated Experimental and Theoretical Study. *Arch. Biochem. Biophys.* **2013**, *539*, 81−86.
(79) Zeida, A.; Babbush, R.; González Lebrero, M. C.; Trujillo, M.; Radi, R.; Estrin, D. A. Molecular Basis of the Mechanism of Thiol Oxidation by Hydrogen Peroxide in Aqueous Solution: Challenging the SN2 Paradigm. *Chem. Res. Toxicol.* **2012**, *25*, 741−746.
(80) Zhao, Y.; Truhlar, D. G. Density Functionals with Broad Applicability in Chemistry. *Acc. Chem. Res.* **2008**, *41*, 157−167.
(81) Eyring, H. The Activated Complex in Chemical Reactions. *J. Chem. Phys.* **1935**, *3*, 107−115.
(82) Pedre, B.; van Bergen, L. A. H.; Pallo, A.; Rosado, L. A.; Dufe, V. T.; Molle, I. V.; Wahni, K.; Erdogan, H.; Alonso, M.; Proft, F. D.; Messens, J.; et al. The Active Site Architecture in Peroxiredoxins: A Case Study on Mycobacterium Tuberculosis AhpE. *Chem. Commun.* **2016**, *52*, 10293−10296.

DOI: 10.1021/acs.jcim.9b00817
J. Chem. Inf. Model. XXXX, XXX, XXX−XXX